

## Phase diagram of one-dimensional electron-phonon systems. II. The molecular-crystal model

Jorge E. Hirsch\*

*Institute for Theoretical Physics, University of California, Santa Barbara, California 93106*

Eduardo Fradkin

*Department of Physics, University of Illinois at Urbana-Champaign, Urbana, Illinois 61801*

(Received 5 November 1982)

We study the nature of the ground state of a one-dimensional electron-phonon model for molecular crystals: The phonons are assumed dispersionless and couple to the local electronic density. We consider the half-filled-band sector and discuss the stability of the Peierls-dimerized ground state as a function of the phonon frequency ( $\omega$ ), electron-phonon coupling constant ( $\lambda$ ), and number of components of the electron spin ( $n$ ). First, we discuss the properties of the model in the limiting cases of zero frequency and infinite frequency. We then perform a strong coupling expansion which maps the system onto a spinless fermion model with nearest-neighbor repulsion for *both* spinless and spin- $\frac{1}{2}$  electrons, but with different parameters in both cases. Finally, we perform a numerical study of the system using a Monte Carlo technique. We study the behavior of the order parameter and of correlation functions for various points in parameter space. We also perform a finite-size-scaling analysis of the numerical data. The conclusions of our study are the following: For the case of spinless electrons, there exists always a disordered phase for small coupling constant, and the system undergoes an infinite-order transition to a Peierls-dimerized state as the coupling constant increases beyond a critical value. The phase diagram is divided between a disordered and an ordered region by a line that connects the points ( $\omega=0, \lambda=0$ ) and ( $\omega=\infty, \lambda=\infty$ ). For the case of spin- $\frac{1}{2}$  electrons, the system is dimerized for arbitrary  $\lambda$  and  $\omega$  except in the limit  $\omega=\infty$ .

### I. INTRODUCTION

This is the second of a series of papers<sup>1</sup> where we discuss the effect of quantum fluctuations on the Peierls instability in one-dimensional electron-phonon systems. In this paper, we study the molecular-crystal model introduced by Holstein<sup>2</sup> to study polarons in molecular crystals. The Hamiltonian is defined by

$$H = \sum_i \left[ \frac{P_i^2}{2M} + \frac{1}{2} K q_i^2 \right] - t \sum_{i,\sigma} (C_{i\sigma}^\dagger C_{i+1,\sigma} + \text{H.c.}) - \lambda \sum_i q_i n_{i\sigma}. \quad (1.1)$$

In this model, the phonons are taken to be dispersionless (Einstein oscillators) and the coupling is to the local electron density  $n_{i\sigma} = C_{i\sigma}^\dagger C_{i\sigma}$ . This model describes vibrations of an internal degree of freedom of a molecule in a one-dimensional molecular crystal. The presence of electrons on the molecule modi-

fies the equilibrium position of the oscillator. The coupling between different oscillators occurs only through mediation by the conduction electrons. These are described by a tight-binding band with nearest-neighbor hopping in Eq. (1.1). More generally, the model Eq. (1.1) can also be viewed as describing the coupling between electrons and excitons with boson character. It has been suggested by Little<sup>3</sup> that this kind of interaction could lead to superconductivity at high temperatures. For the case studied in this paper, however, the Peierls instability dominates and eliminates the possibility of superconducting correlations even at high oscillator frequency. This is due to the fact that we consider the half-filled-band case where umklapp scattering is dominant. Within mean-field theory the system Eq. (1.1) is unstable against a lattice distortion into a Peierls-dimerized state.<sup>4</sup> The purpose of this paper is to discuss how the mean-field results (which are exact in the limit  $M = \infty$ ) are modified for finite  $M$  when the quantum fluctuations of the phonon field are taken into consideration.

In a recent paper we discussed the same questions for the one-dimensional Su-Schrieffer-Heeger (SSH) model<sup>5</sup> for electron-phonon interactions.<sup>1</sup> That model (introduced by these authors to describe polyacetylene) is defined by the Hamiltonian

$$H = \sum_i \left[ \frac{P_i^2}{2M} + \frac{1}{2} K (q_{i+1} - q_i)^2 \right] - \sum_{i,\sigma} [t - \lambda(q_{i+1} - q_i)] (C_{i\sigma}^\dagger C_{i+1\sigma} + \text{H.c.}) . \quad (1.2)$$

Here the phonon degrees of freedom are longitudinal lattice vibrations and the coupling to the electrons is through modification of the electron-hopping matrix elements. A more general model for a quasi-one-dimensional solid (for example, organic charge-transfer compounds) would involve both types of vibrational degrees of freedom described by (1.1) and (1.2),<sup>6</sup> but we have not attempted such a study here. In a recent paper, Campbell *et al.*<sup>7</sup> compare the properties of polarons in the models Eqs. (1.1) and (1.2).

The models Eqs. (1.1) and (1.2) are defined by two parameters as far as ground-state properties are concerned which we can take to be the electron-phonon coupling constant  $\lambda$  and phonon frequency  $\omega = \sqrt{K/M}$ . The parameters  $t$  and  $K$  can be set equal to 1 by redefining the overall energy scale and the units of phonon displacement. The two models have identical properties in the  $\omega=0$  limit and within mean-field theory: The ground state is dimerized for an arbitrary electron-phonon coupling constant. The electronic spin plays no particular role in this limit except for defining an effective coupling  $\lambda_{\text{eff}} = \sqrt{n} \lambda$  ( $n=1$  for spinless electrons and  $n=2$  for spin- $\frac{1}{2}$  electrons). In this limit the two models differ only in that the electronic charge-density wave (CDW) resides on the sites for the molecular-crystal model and on the bonds for the SSH model. However, the behavior in the opposite limit,  $\omega = \infty$ , is quite different. In that limit the molecular-crystal model has no long-range order for arbitrary coupling for both  $n=1$  and 2. In contrast, the SSH model is dimerized for arbitrary coupling if  $n=2$  and becomes dimerized for coupling stronger than a critical value in the case  $n=1$ . For intermediate values of the mass we find the behavior of both models to be qualitatively similar: For  $n=1$ , a disordered region for a small coupling constant and an infinite-order transition to a Peierls-dimerized state for a critical value of  $\lambda$ , and for  $n=2$ , a dimerized phase for arbitrary nonzero  $\lambda$ . As discussed in Ref. 1, the reason for the different behavior of the cases  $n=1$  and 2 is the umklapp scattering between

conduction electrons induced by phonon fluctuations: For  $n=2$  the umklapp scattering opens up a gap in the electronic spectrum and gives long-range dimerization order. In contrast, for  $n=1$  the umklapp scattering is not effective in opening up a gap for small coupling constant because of the Pauli exclusion principle, and only becomes relevant for the coupling exceeding a critical value. This has been recently pointed out by several authors for models of interacting spinless fermions.<sup>8-10</sup>

An attractive feature of the model Eq. (1.1) is that it has a well-behaved strong coupling limit. In that limit the system behaves as a narrow band of small polarons.<sup>11</sup> We have carried out a strong coupling expansion to find the interactions between the polarons. A similar expansion was carried out by Beni *et al.*<sup>12</sup> for a related model. This expansion maps the model onto a spinless fermion model with nearest-neighbor repulsions (or equivalently an anti-ferromagnetic *XXZ* model)<sup>13</sup> for both  $n=1$  and 2, but with different parameters in both cases. This allows us to obtain an analytic form for the critical coupling  $\lambda_c$  as a function of the ionic frequency in strong coupling for the case  $n=1$ .

We have also performed an extensive numerical study of this model with the use of a Monte Carlo (MC) technique.<sup>14,15</sup> Recently, Scalapino and Sugar have studied certain properties of this model for  $n=1$  with the use of another MC technique.<sup>16</sup> However, that method was slow so that only small systems could be studied. The present numerical procedure allows us to get quantitative results for lattice and electronic properties for large lattices, since the computation time increases only linearly with the size of the lattice, for arbitrary parameters. Typically, 40-site rings were studied. The numerical results appear to indicate that the model for  $n=2$  is always dimerized at a finite phonon frequency. However, we cannot rule out from the numerical data the possibility of having a disordered phase for small coupling constant and high ionic frequency. We cannot distinguish from the MC data a disordered region from an ordered region where the correlation length is much larger than the lattice studied. We have carried out a finite-size-scaling analysis of the numerical data for one case, which appears to indicate that the system does not disorder for  $n=2$ . From the theoretical arguments in conjunction with the numerical data we conclude that there is strong evidence that the system for  $n=2$  is always dimerized at a finite phonon frequency. For the case  $n=1$  our numerical results for the location of the phase-transition point approach the analytic results for strong coupling.

This paper is organized as follows. In Sec. II we review the properties of this model in the  $\omega=0$  lim-

it. In Sec. III we analyze the properties of the model in the  $\omega = \infty$  limit. It is shown that the spinless model is equivalent to free fermions and thus has no long-range order. The spin- $\frac{1}{2}$  case is equivalent to an attractive Hubbard model in that limit. The properties of that model are discussed by analyzing its location in the phase diagram of the one-dimensional electron gas obtained from weak coupling renormalization-group calculations ("gology")<sup>17</sup>: The attractive Hubbard model lies right on the boundary between a region of CDW long-range order and singlet-superconductivity (SS) algebraic order. It is also shown that this model has a continuous symmetry that prevents CDW formation. However, retardation breaks this continuous symmetry down to a discrete symmetry so that CDW order becomes possible when the phonon frequency is finite. In Sec. IV we perform a strong coupling expansion for the molecular-crystal model. For the case  $n = 2$ , the results of this expansion indicate that the system is always dimerized for  $\omega < \infty$  in this regime ( $\lambda/\sqrt{Kt} \gg 1$ ). For the case  $n = 1$ , as mentioned earlier, one obtains a phase-transition line. In Sec. V we discuss results of MC simulations of the model. Besides confirming the results of the analytic calculations in the various limits, the numerical results give us quantitative information for intermediate regions in parameter space. We conclude in Sec. VI with a short discussion. Future studies of these models will include consideration of the effect of adding electron-electron interactions in the Hamiltonian Eqs. (1.1) and (1.2). It will also be of interest to study a model where both types of phonons are present simultaneously. (Part of the results presented in this paper were reported briefly elsewhere.<sup>15</sup>)

## II. $\omega = 0$ LIMIT

Before we begin our discussion, it is useful to rewrite the model Eq. (1.1) as

$$H = \sum_i \left[ \frac{P_i^2}{2M} + \frac{1}{2} K q_i^2 \right] - t \sum_{i,\sigma} (C_{i\sigma}^\dagger C_{i+1,\sigma} + \text{H.c.}) - \lambda \sum_{i,\sigma} q_i (n_{i\sigma} - \frac{1}{2}). \quad (2.1)$$

In going from (1.1) to (2.1) we have simply redefined the equilibrium position of the oscillators and added a chemical potential appropriate to the half-filled-band case to Eq. (1.1). The model Eq. (2.1) has now explicit particle-hole symmetry since the transformation  $C_{i\sigma} \rightarrow (-1)^j C_{i\sigma}^\dagger$ ,  $q_i \rightarrow -q_i$ , leaves the Hamiltonian invariant.

The properties of the model Eq. (2.1) in the static limit are similar to those of the SSH model. As-

sume the molecular distortions have the form

$$q_i = (-1)^i m_p, \quad (2.2)$$

with  $m_p$  the phonon-staggered order parameter. The value of  $m_p$  that minimizes the total ground-state energy satisfies the equation

$$1 = \frac{\lambda^2 n}{2\pi K} \int_0^\pi \frac{dk}{(\epsilon_k^2 + \Delta^2)^{1/2}} \quad (2.3)$$

for an infinite system, with  $\epsilon_k = -2t \cos k$  being the electron band energy and  $\Delta = m_p \lambda$  being the electronic energy gap. Equation (2.3) has a nonzero solution for  $\Delta$  for an arbitrary coupling constant. In the limit of small  $\lambda$ , one finds

$$\Delta = 8t e^{-(2\pi K t / n \lambda^2)}. \quad (2.4)$$

The electrons form a CDW and the electronic order parameter is defined as

$$m_e = \frac{1}{N} \sum_{j=1}^N \sum_{\sigma=1}^n (-1)^j \langle 0 | n_{j\sigma} | 0 \rangle, \quad (2.5)$$

with  $|0\rangle$  the ground state of the system. Equation (2.5) defines a CDW defined on the sites, in contrast to the SSH model where the CDW resides on the bonds. The electronic order parameter is related to the phonon order parameter by

$$m_e = \frac{K}{\lambda} m_p$$

in the  $\omega = 0$  limit, or equivalently within self-consistent mean-field theory. It is clear from Eq. (2.4) that in this limit the system has dimerization long-range order and a gap in the spectrum for arbitrary electron-phonon coupling constant  $\lambda$ . The number of components of the electron spin  $n$  enters only in defining an effective electron-phonon coupling constant  $\lambda_{\text{eff}} = \sqrt{n} \lambda$  in Eq. (2.4). In the following sections we will study how quantum fluctuations modify these results.

## III. $\omega = \infty$ LIMIT

We consider now the opposite limit, where the phonon frequency goes to infinity. This is not such an unphysical limit as it may seem at first sight. It is usually assumed that the hopping matrix elements in the tetracyanoquinodimethane (TCNQ) salts are in the range of  $10^{-1}$  to  $10^{-2}$  eV, which is comparable to characteristic molecular vibration energies. Furthermore, for systems where the boson degrees of freedom are *excitonic* rather than vibrational, characteristic frequencies could be much higher, of the order of 1 eV. To study the properties of our model in this limit, it is useful to rewrite the problem in a functional integral formulation. The partition function is given by

$$Z = \int \prod_j \mathcal{D}q_j(\tau) \text{Tr} T_\tau \exp - \int_0^\beta d\tau \sum_j \left[ \frac{1}{2} M \dot{q}_j^2(\tau) + \frac{1}{2} K q_j^2(\tau) - t \sum_\sigma [C_{j\sigma}^\dagger(\tau) C_{j+1,\sigma}(\tau) + \text{H.c.}] + \lambda q_j(\tau) \sum_\sigma [n_{j\sigma}(\tau) - \frac{1}{2}] \right]. \quad (3.1)$$

In Eq. (3.1), we have written the phonon part as a functional integral and kept the electronic part as a trace over operators. The symbol  $T_\tau$  stands for time ordering, with earlier times to the left. We can now integrate over the phonon degrees of freedom and obtain

$$Z = \text{Tr} T_\tau \exp - \left[ \int_0^\beta d\tau \left[ -t \sum_{j,\sigma} [C_{j\sigma}^\dagger(\tau) C_{j+1,\sigma}(\tau) + \text{H.c.}] - \frac{\lambda^2}{2K} \int_0^\beta d\tau \int_0^\beta d\tau' \sum_{j,\sigma,\sigma'} [n_{j\sigma}(\tau) - \frac{1}{2}] G(\tau\tau') (n_{j\sigma'} - \frac{1}{2}) \right] \right], \quad (3.2)$$

where the phonon Green's function is given by

$$G(\tau, \tau') = \frac{\omega}{2} e^{-\omega|\tau-\tau'|}. \quad (3.3)$$

Equation (3.2) defines an effective interaction for the electrons which is nonlocal in time. However, in the  $\omega \rightarrow \infty$  limit one obtains

$$G(\tau, \tau') \xrightarrow{\omega \rightarrow \infty} \delta(\tau - \tau'), \quad (3.4)$$

and the interactions in (3.2) become instantaneous. Equation (3.2) then defines an effective Hamiltonian of the form:

$$H_{\text{eff}} = -t \sum_{j,\sigma} (C_{j\sigma}^\dagger C_{j+1,\sigma} + \text{H.c.}) - \frac{\lambda^2}{2K} \sum_{j,\sigma,\sigma'} (n_{j\sigma} - \frac{1}{2})(n_{j\sigma'} - \frac{1}{2}). \quad (3.5)$$

In the case  $n = 1$ , Eq. (3.5) reduces to

$$H_{\text{eff}} = -t \sum_j (C_j^\dagger C_{j+1} + \text{H.c.}) - \frac{\lambda^2}{8K} \sum_j 1 \quad (3.6)$$

by using the property  $n_j n_j = n_j$ . Thus one obtains a Hamiltonian for free electrons in this limit. This has been previously pointed out by Scalapino and Sugar.<sup>16</sup> The system is then undimerized for arbitrary electron-phonon coupling constant. For large  $\lambda$ , the phonons follow the movement of the electrons in what can be described as a small-polaron band. The bandwidth is unrenormalized in this limit. This will be discussed in more detail in the following section.

In the case  $n = 2$ , we obtain, from Eq. (3.5),

$$H_{\text{eff}} = -t \sum_{j,\sigma} (C_j^\dagger C_{j+1,\sigma} + \text{H.c.}) - \frac{\lambda^2}{K} \sum_j n_{j\uparrow} n_{j\downarrow} + \frac{\lambda^2}{2K} \sum_{j,\sigma} n_{j\sigma} - \frac{\lambda^2}{2K} \sum_j 1. \quad (3.7)$$

Equation (3.7) defines an attractive Hubbard model with an interaction

$$U = -\lambda^2 / K.$$

This model has a gap in the spin-density-wave spectrum but no gap in the CDW spectrum. The ground state does not have long-range order for any value of  $U$ . The properties of this model for arbitrary  $U$  can be inferred from several studies. First, Lieb and Wu<sup>18</sup> have shown that there is no singularity in the Hubbard model except possibly at  $U = 0$ . Thus the properties of the model for all  $U < 0$  can be expected to be the same. For small  $U$  we can obtain the properties of the model from the  $g$ -ology phase diagram obtained from weak coupling renormalization-group (RG) calculations.<sup>17</sup> The couplings for the model Eq. (3.7) are

$$g_1 = g_2 = g_3 = -\frac{\lambda^2}{2K}, \quad (3.8)$$

with  $g_1$ ,  $g_2$ , and  $g_3$  being the interactions for backward, forward, and umklapp scattering, respectively. The  $g$ -ology phase diagram in the half-filled-band sector is shown in Fig. 1. The attractive Hubbard model lies right on the dividing line between the CDW and SS regions. On that line it can be shown from the RG recursion relations that electron

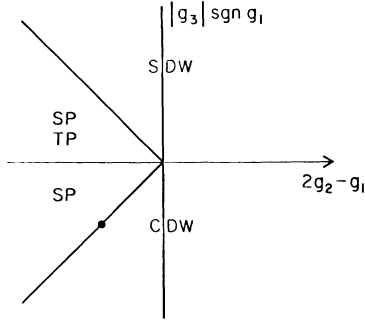


FIG. 1. Phase diagram in the half-filled-band sector from weak coupling renormalization group (Ref. 16). Region labeled CDW has long-range charge-density-wave order in the ground state. Regions labeled SDW, SP, and TP have algebraic order in the spin-density-wave, singlet-pairing, and triplet-pairing correlation functions, respectively. Attractive Hubbard model (dot) lies on the boundary between the CDW and SP regions.

charge-density correlations decay as

$$\langle n_{0n_R} \rangle \sim 1/R, \quad (3.9)$$

in contrast to the case of free electrons where they decay as  $1/R^2$ . The system is at the critical point for this case.

It is easy to see quite generally that the attractive Hubbard model cannot have long-range order in the charge degrees of freedom. Consider the following transformation<sup>17</sup>:

$$\begin{aligned} C_{i\uparrow} &= d_{i\uparrow}, \\ C_{i\downarrow} &= (-1)^i d_{i\downarrow}^\dagger. \end{aligned} \quad (3.10)$$

This transformation leaves the hopping part of the Hamiltonian (3.7) invariant and changes the sign of the interaction. It also interchanges the role of charge and spin degrees of freedom. The resulting repulsive Hubbard model, although it has short-ranged antiferromagnetic correlations, does not have long-range order in the spin degrees of freedom. The reason is that it has a continuous-symmetry rotation in spin space which cannot be broken spontaneously in two dimensions due to the Mermin-Wagner theorem.<sup>19</sup> The corresponding continuous symmetry in the *attractive* Hubbard model Eq. (3.7) is, with the use of (3.10),

$$\begin{aligned} \tilde{C}_{i\uparrow} &= \cos\theta C_{i\uparrow} + (-1)^i \sin\theta C_{i\downarrow}^\dagger, \\ \tilde{C}_{i\downarrow} &= -(-1)^i \sin\theta C_{i\uparrow}^\dagger + \cos\theta C_{i\downarrow}. \end{aligned} \quad (3.11)$$

It is easy to verify that the transformation (3.11) leaves the Hamiltonian (3.7) invariant. Furthermore, a dimerization order parameter, of the form

$$m_e = (-1)^i \langle n_{i\uparrow} + n_{i\downarrow} \rangle, \quad (3.12)$$

would break the continuous-symmetry equation (3.11). This is most easily seen through the transformation (3.10), since the transformed order parameter is

$$m_e^T = (-1)^i \langle n_{i\uparrow} - n_{i\downarrow} \rangle, \quad (3.13)$$

which clearly breaks the rotational symmetry in spin space. Thus we conclude that the continuous-symmetry equation (3.11) prevents the existence of long-range dimerization order in the molecular-crystal model when  $\omega \rightarrow \infty$  for  $n=2$ .

The importance of the above considerations resides in the fact that a finite frequency  $\omega < \infty$  breaks the continuous-symmetry equation (3.11) down to a discrete symmetry. In a short-time expansion of (3.2) in powers of the inverse frequency, one generates terms of the form

$$\frac{\lambda^2 t}{K\omega} (n_{j\uparrow} + n_{j\downarrow}) [H_0, n_{j\uparrow} + n_{j\downarrow}],$$

which are not invariant under the transformation (3.11). Thus we conclude from this section that retardation effects can produce dimerization in the case  $n=2$  for any  $\omega < \infty$ . This will be shown to be the case at least in the strong-coupling regime in the following section.

In contrast to the molecular-crystal model, the SSH model [Eq. (1.2)] has long-range dimerization order for arbitrary  $\lambda$  even for  $\omega = \infty$  in the case  $n=2$ .<sup>1</sup> This may seem surprising since the transformation Eq. (3.11) leaves also the SSH Hamiltonian invariant (in the SSH case that happens also for finite  $\omega$ ). However, the dimerization order parameter in that case is

$$m_e = (-1)^i \langle C_{i\sigma}^\dagger C_{i+1\sigma} + \text{H.c.} \rangle, \quad (3.14)$$

and it is easy to verify that this order parameter does not break the continuous-symmetry equation (3.11).

#### IV. STRONG COUPLING EXPANSION

In this section we consider an expansion of the Hamiltonian (2.1) in powers of the hopping matrix element  $t$ . The expansion is somewhat different for the cases  $n=1$  and 2, so we discuss them separately.

##### A. Spinless electrons

We take as unperturbed Hamiltonian,

$$H_0 = \sum_i \left[ \frac{P_i^2}{2M} + \frac{1}{2} K q_i^2 \right] - \lambda \sum_i q_i (n_i - \frac{1}{2}) \equiv \sum_i H_i. \quad (4.1)$$

The Hamiltonian for a site can be written as

$$H_i = \frac{P_i^2}{2M} + \frac{1}{2}K \left[ q_i + \frac{\lambda}{K} \left( n_i - \frac{1}{2} \right) \right]^2 - \frac{\lambda^2}{2K}. \quad (4.2)$$

Thus the presence or absence of an electron at site  $i$  simply shifts the equilibrium position of the oscillator to  $+q_0$  or  $-q_0$ , with

$$q_0 = \lambda/2K. \quad (4.3)$$

We will denote by  $|+n\rangle$  and  $|-n\rangle$  the  $n$ th excited state of the oscillator with equilibrium position  $+q_0$  and no electron at the site and with  $-q_0$  and one electron at the site, respectively. In zeroth order the ground state of (4.1) is highly degenerate: We simply have to distribute  $N/2$  electrons over  $N$  sites; the energy is independent of which sites are occupied. The perturbation

$$H_1 = -t \sum_i (C_i^\dagger C_{i+1} + C_{i+1}^\dagger C_i) \quad (4.4)$$

breaks this degeneracy in first order, forming a band of small polarons. It is clear that  $H_1$  will have nonzero matrix elements between states where an electron goes from site  $i$  to  $i+1$ , and the equilibrium positions of the oscillators shift accordingly. The matrix element of  $H_1$  is proportional to the

overlap between the two oscillator ground states,

$$\begin{aligned} \langle +0 | -0 \rangle &= e^{-g}, \\ g &= \frac{\lambda^2}{4K\omega}, \end{aligned} \quad (4.5)$$

so that to first order one obtains a small-polaron band with hopping matrix element

$$\tilde{t} = t e^{-2g}. \quad (4.6)$$

In second order, the effective Hamiltonian can be written as

$$H_2 = \sum_\alpha \frac{|i\rangle\langle i| H_1 |\alpha\rangle\langle\alpha| H_1 |j\rangle\langle j|}{E_i - E_\alpha}, \quad (4.7)$$

where  $\alpha$  denotes intermediate states that are not part of the degenerate manifold of ground states of  $H_0$ , i.e., where the oscillators are in excited states. There are two types of second-order processes: one where an electron hops to a neighboring site and back to the same site, which gives a nearest-neighbor repulsion term between polarons. In the second process an electron hops from one site to its nearest neighbor and then to its second-nearest neighbor. The details of the calculation are given in the Appendix. The resulting second-order Hamiltonian is

$$H_{\text{eff}} = -\tilde{t} \sum_i (\tilde{C}_i^\dagger \tilde{C}_{i+1} + \tilde{C}_{i+1}^\dagger \tilde{C}_i) + \tilde{V} \sum_i \tilde{n}_i \tilde{n}_{i+1} + \tilde{t}_2 \sum_i [\tilde{C}_{i+1}^\dagger (1 - \tilde{n}_i) \tilde{C}_{i-1} + \tilde{C}_{i-1}^\dagger (1 - \tilde{n}_i) \tilde{C}_{i+1}], \quad (4.8)$$

where the operator  $\tilde{C}_i^\dagger$  creates an electron at site  $i$  and changes the oscillator ground state from being centered at  $q_0$  to  $-q_0$ . The parameters in (4.8) are given by

$$\tilde{V} = 2 \frac{\tilde{t}^2}{\omega} \int_0^g dg' \frac{e^{4g'} - 1}{g'}, \quad (4.9a)$$

$$\tilde{t}_2 = \frac{\tilde{t}^2}{\omega} \int_0^g dg' \frac{e^{2g'} - 1}{g'}. \quad (4.9b)$$

As  $\omega \rightarrow \infty$  we obtain  $\tilde{V}, \tilde{t}_2 \rightarrow 0$ , and  $\tilde{t} \rightarrow t$ , and we recover the results of the preceding section, a free-electron band. For large  $g$  we obtain

$$\tilde{V} \sim \frac{t^2}{2\omega g}, \quad (4.10a)$$

$$\tilde{t}_2 = \tilde{t} \frac{t}{2\omega g}. \quad (4.10b)$$

Note that  $\tilde{t}_2/\tilde{t}$  becomes very small as  $g$  increases and we will neglect it in what follows. As  $g$  grows the hopping term in Eq. (4.8) decreases exponentially while the nearest-neighbor repulsion term decreases algebraically, so that it will eventually dominate. In fact, it is well known that the Hamiltonian (4.8)

[with the next-nearest-neighbor (NNN) hopping neglected] undergoes an infinite-order transition to a CDW state at the point

$$\frac{\tilde{V}_c}{2\tilde{t}} = 1.$$

This is easily established by mapping (4.8) through a Jordan-Wigner transformation<sup>20</sup> to the antiferromagnetic  $XXZ$  Hamiltonian. The transition point corresponds to the isotropic Heisenberg point.

To summarize this subsection the strong coupling expansion in the spinless case yields a phase boundary between a disordered and a Peierls-dimerized phase for values of  $\lambda$  and  $\omega$  satisfying

$$\frac{t e^{-2g}}{\omega} \int_0^g dg' \frac{e^{4g'} - 1}{g'} = 1, \quad (4.11)$$

with  $g$  given by (4.5). This expansion should be valid in the region  $\lambda^2/Kt \gg 1$ .

### B. Spin- $\frac{1}{2}$ electrons

The site Hamiltonian is now

$$H_i = \frac{P_i^2}{2M} + \frac{1}{2}K \left[ q_i + \frac{\lambda}{K}(n_{i\uparrow} + n_{i\downarrow} - 1) \right]^2 - \frac{\lambda^2}{2K}(n_{i\uparrow} + n_{i\downarrow} - 1)^2. \quad (4.12)$$

Note that the lowest energy corresponds to the site being either empty or doubly occupied; the singly occupied sites have a higher energy. This is due to the fact that the phonons produce an attraction between the electrons and that we chose the chemical potential to correspond to a half-filled band. The ground state of the unperturbed Hamiltonian consists now in distributing  $N/2$  pairs of electrons between the  $N$  sites, and the oscillator equilibrium positions are now  $\pm q_0$ , with  $q_0 = \lambda/K$  for empty and doubly occupied sites, respectively.

The main difference between this case and the case of spinless electrons resides in that in this case we do not obtain any contribution from the hopping term in first order. The reason is that the hopping term breaks pairs in first order and the resulting state is not part of the ground-state manifold. In second order we have two processes: a nearest-neighbor hopping term for the pairs and a nearest-neighbor repulsion between pairs. The effective Hamiltonian to second order is again of the form

$$H = -\tilde{t} \sum_i (\tilde{b}_i^\dagger \tilde{b}_{i+1} + \text{H.c.}) + \tilde{V} \sum_i \tilde{n}_i \tilde{n}_{i+1}, \quad (4.13)$$

where  $\tilde{b}_i$  creates a pair of electrons at site  $i$  and shifts the oscillator equilibrium position from  $-q_0$

$$\begin{aligned} Z = & \int \prod dq_{ij} \exp \left[ - \sum_{i=1}^L \sum_{j=1}^N \left[ \frac{1}{2} M \frac{(q_{i+1,j} - q_{i,j})^2}{\Delta\tau} + \frac{1}{2} K q_{ij}^2 \Delta\tau \right] \right] \\ & \times \text{Tr} \sum_{i=1}^L \exp \left[ - \Delta\tau \lambda \sum_{j\sigma} q_{ij} (n_{j\sigma} - \frac{1}{2}) \right] \exp \left[ \Delta\tau t \sum_{\substack{j \text{ even} \\ \sigma}} (C_{j\sigma}^\dagger C_{j+1\sigma} + \text{H.c.}) \right] \\ & \times \exp \left[ \Delta\tau t \sum_{\substack{j \text{ odd} \\ \sigma}} (C_{j\sigma}^\dagger C_{j+1\sigma} + \text{H.c.}) \right], \end{aligned} \quad (5.1)$$

where  $1 \leq j \leq N$  labels spatial position on an  $N$ -site ring and  $1 \leq i \leq L$  labels imaginary time. Upon insertion of complete sets of intermediate states for the electrons in the occupation-number representa-

tion, one obtains a classical system defined on a checkerboard space-time lattice. We stress that our procedure is exact, except for terms of order  $\Delta\tau^2$  times commutators of different parts of the Hamil-

$$\tilde{t} = 2 \frac{t^2}{\omega} e^{-4g} \sum_{nn'} (-1)^{n+n'} \frac{(2g)^{n+n'}}{n!n'} \frac{1}{n+n'+4g}, \quad (4.14a)$$

$$\tilde{V} = 4 \frac{t^2}{\omega} e^{-4g} \sum_{nn'} \frac{(2g)^{n+n'}}{n!n'} \frac{1}{n+n'+4g}. \quad (4.14b)$$

The derivation of (4.13) and (4.14) is given in the Appendix. Note that

$$\frac{\tilde{V}}{2\tilde{t}} \geq 1,$$

the equality being achieved only for  $\omega = \infty$  where only the  $n = n' = 0$  term in (4.14) contributes. At that point, the Hamiltonian (4.13) is at its critical point and has no long-range order. This is in accordance with the results of the  $\omega = \infty$  analysis of Sec. III. In fact, Emery<sup>21</sup> has shown that the attractive Hubbard model Eq. (3.7) can be mapped onto the model (4.13) with  $\tilde{V} = 2\tilde{t} = Kt^2/\lambda^2$  in strong coupling. For  $\omega < \infty$ , one can see from (4.14) that  $\tilde{V}/2\tilde{t} > 1$ , and the system Eq. (4.13) has long-range order with a CDW of period 2 in the ground state. Thus, in contrast to the  $n = 1$  case, we find that for  $n = 2$  the system is dimerized for *arbitrary* finite frequency in strong coupling.

### V. NUMERICAL SIMULATIONS

In this section we present results of MC simulations of the molecular-crystal model. The numerical method has been described in detail in Ref. 14. The partition function is written as

tion, one obtains a classical system defined on a checkerboard space-time lattice. We stress that our procedure is exact, except for terms of order  $\Delta\tau^2$  times commutators of different parts of the Hamil-

tonian, which have been neglected in obtaining Eq. (5.1). To eliminate these errors one should take  $\Delta\tau t \ll 1$ ,  $\Delta\tau\omega \ll 1$ . However, the number of time slices  $L$  needed for a given temperature increases when  $\Delta\tau$  decreases ( $\beta=L\Delta\tau$ ), and the number of sweeps necessary to obtain good statistics increases with  $\Delta\tau$  [roughly as  $1/(\Delta\tau)^2$ ] since the acceptance fraction for the fermion moves decreases. In our simulations we took typically  $\Delta\tau=0.5$  for  $0 \leq \omega \leq 1$  and  $\Delta\tau=0.25$  for  $1 < \omega \leq 2$ . This produces errors of a few percent (we take units so that  $t=1$  and  $K=0.25$  throughout this section). We also need to be at low enough temperatures since we want to study ground-state properties. We have found that taking square lattices ( $N=L$ ) for  $\Delta\tau \geq 0.25$  produced no noticeable thermal fluctuations in the system, indicating that the thermal correlation length is much larger than the lattice.

The MC procedure consists in going sequentially through the space-time lattice and updating the fermion-world lines and the phonon field at each point. For updating the phonon field we chose a step size  $\delta$  and attempted to change the field  $q_{ij}$  to  $q_{ij} + r\delta$ , with  $r$  a random number between  $-1$  and  $1$ . The move was accepted or rejected according to the standard Metropolis algorithm. The step size  $\delta$  was chosen so that the fraction of accepted moves was about  $0.5$ . Furthermore, several attempts (3–6) were made to update the phonon field at a given site, to bring it in equilibrium with its surroundings. For the updating of the fermion-world lines we followed the procedure described in Ref. 14. In addition to changing both fields separately we have also allowed for moves where the fermion is moved (or a pair of fermions at the same site in the case  $n=2$ ) and at the same time the phonon coordinate is changed to  $(-)$  itself. These composite moves become dominant in the strong coupling high-frequency limit (small-polaron regime). It can be seen from Eq. (5.1) that the cost in action in changing  $n_{j\sigma}$  to  $1-n_{j\sigma}$  and at the same  $q_{ij}$  to  $-q_{ij}$  is independent of  $\lambda$ . The cost in the phonon action for that move is determined solely by the ion mass and it vanishes as  $M \rightarrow 0$ . Thus it is easy to see from (5.1) that the system will disorder as  $M \rightarrow 0$ , as was discussed in Sec. III.

Figure 2 shows a typical field configuration for the case  $n=2$ , with  $\omega=1.1$ ,  $\lambda=1/\sqrt{2}$ . Note that the electrons [Fig. 2(a)] are almost always paired and that they form a well-ordered CDW even though the phonon frequency is fairly large (the adiabatic gap for this case is  $\Delta=1.54$ ). The staggered-phonon field [Fig. 2(b)] shows that the system is well dimerized for these parameters with occasional quantum fluctuations to the opposite phase. In contrast, we show in Fig. 3 a typical field configuration for the

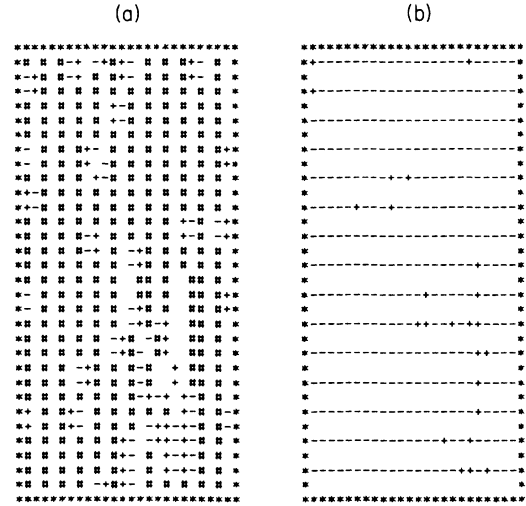


FIG. 2. Typical configuration of the electron and phonon fields for a 24-site ring for  $n=2$ ,  $\omega=1.1$ , and  $\lambda=1/\sqrt{2}$ . (a) Electron configuration is denoted by  $+$  ( $-$ ) for spin up (down) and  $\#$  for double occupation. (b) Sign of the staggered-phonon field. Note that the system is well ordered.

case  $n=1$ ,  $\omega=1.1$ . To make a comparison with the  $n=2$  case we have taken a coupling constant that is  $\sqrt{2}$  times bigger than in Fig. 2, i.e.,  $\lambda=1$ . In the static limit both cases would have the same gap since the combination  $n\lambda^2$  enters in Eq. (2.4). Note that here the fluctuations are much bigger and the system appears to be in a disordered state. The phonon-field configuration shows fairly wide re-

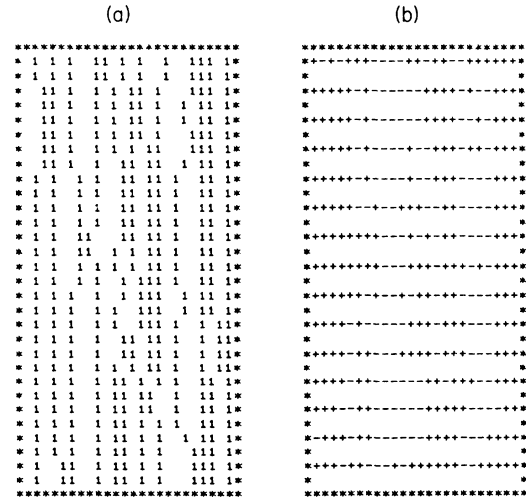


FIG. 3. Same as Fig. 2 for the case  $n=1$ ,  $\omega=1.1$ , and  $\lambda=1$ . Electron is denoted by  $1$  here. Note that fluctuations are much larger here than in Fig. 2.

gions where the system is in one of the dimerized ground states separated by solitons from each other. It can already be seen from these pictures that the case of spinless electrons ( $n=1$ ) is much more sensitive to quantum fluctuations than the  $n=2$  case.

Figures 4 and 5 show the phonon order parameter as a function of  $\lambda$  for three different values of the phonon frequency:  $\omega=0.41, 1.1,$  and  $2$  for the cases  $n=1$  and  $2$ . For these and the following runs  $40 \times 40$  systems were used. In Figs. 4 and 5, the sys-

tem was started at  $\lambda=0$ , and  $\lambda$  was increased very slowly up to the maximum value and then decreased slowly to zero. Typically, 500 values of  $\lambda$  were taken between 0 and the maximum value, and at each point the results of four measurements separated by four passes were averaged. If the rate of increase in  $\lambda$  was not small enough, the system became ordered with some frozen-in defects and usually it could not get rid of them until the coupling constant was again small. The smooth curves in Figs. 4 and 5 are

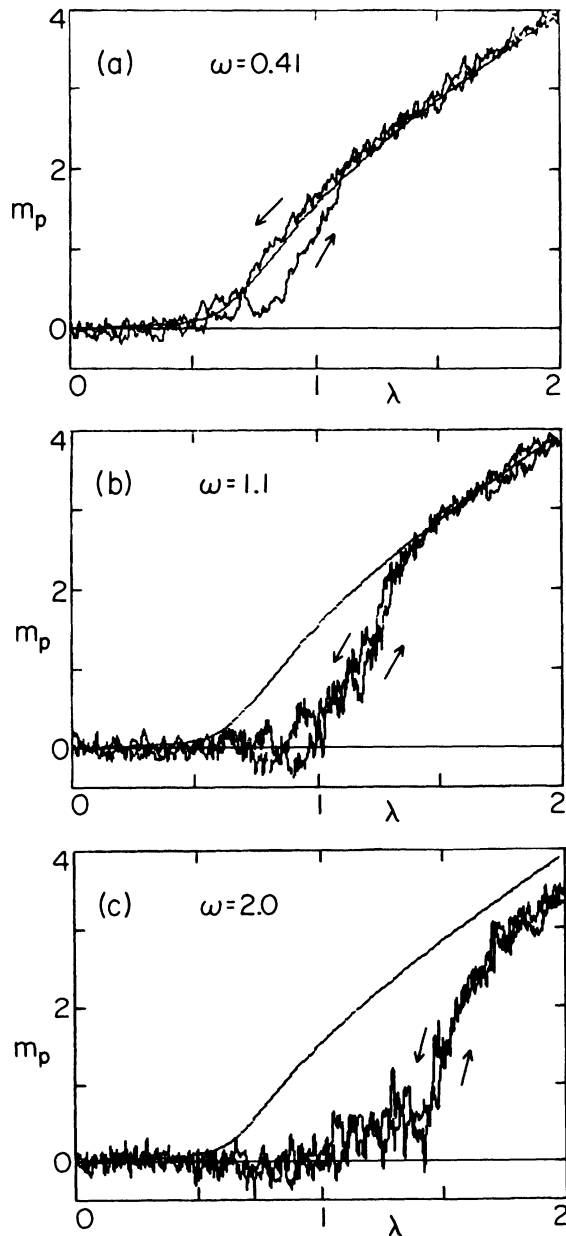


FIG. 4. Phonon order parameter vs  $\lambda$  for the case  $n=1$  and three values of  $\omega$ . Smooth lines are the  $\omega=0$  exact results.

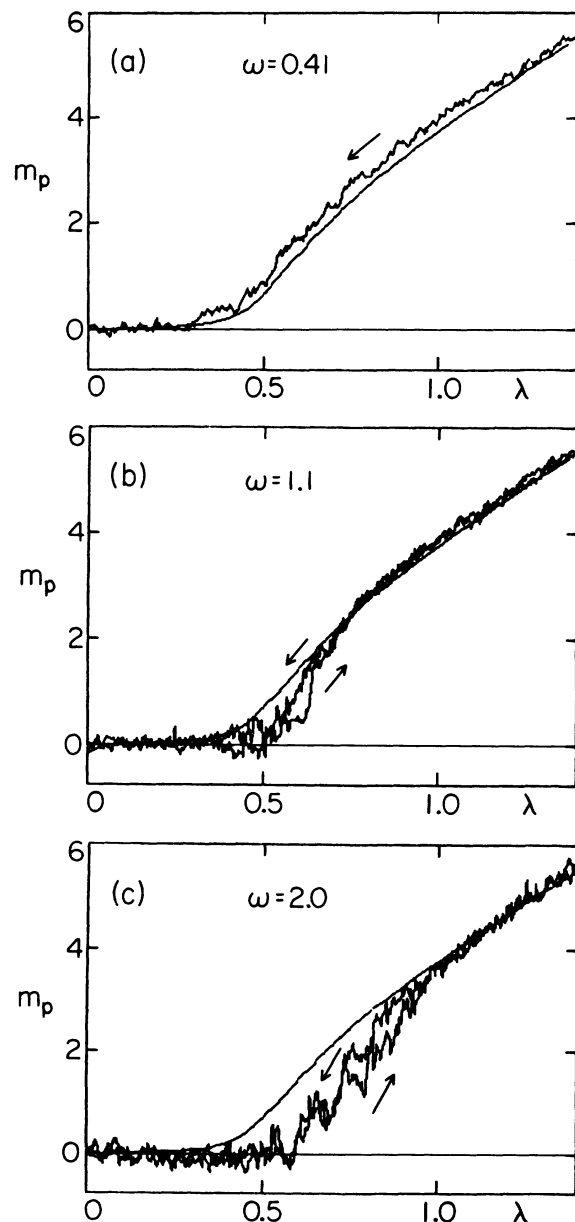


FIG. 5. Phonon order parameter vs  $\lambda$  for the case  $n=2$  and three values of  $\omega$ . Smooth lines are the  $\omega=0$  results.

the results for the  $40 \times 40$  lattice in the static limit.

Figure 4 shows the case  $n=1$ . In Fig. 4(a) ( $\omega=0.41$ ), results are still the same as for  $\omega=0$  within errors. The hysteresis loop is due to some defects which became temporarily frozen in as  $\lambda$  was increased. We always obtained hysteresis loops for both  $n=1$  and 2 if the change in  $\lambda$  was too fast. We do not believe, however, that these should be taken as an indication of a phase transition, but that they occur around the cross-over region where the correlation length becomes smaller than the lattice.

Figure 4(b) shows results for  $\omega=1.1$ . Here, we see already a substantial deviation from the  $\omega=0$  results. We believe that a phase transition occurs in this case for  $\lambda \sim 0.9$  to 1. We will return to this case later in this section. Figure 4(c) shows the case  $\omega=2$ . Here, the system seems to undergo a transition around  $\lambda \sim 1.4$ . To summarize, Fig. 4 appears to indicate that the system for  $n=1$  undergoes a transition from an undimerized to a dimerized phase at a critical coupling  $\lambda_c$  which increases as  $\omega$  increases.

Figure 5 shows the corresponding results for  $n=2$ . Note that we have chosen the horizontal scale different,  $0 \leq \lambda \leq 2$ , for Fig. 4, and  $0 \leq \lambda \leq 1.4$  for Fig. 5. Again, the reason was that within mean-field theory the effective coupling constant is  $\sqrt{n} \lambda$ . In Fig. 5 ( $\omega=0.41$ ) we only show the results starting from an ordered configuration and going down in  $\lambda$ . We were unable to get the system to dimerize completely starting from a disordered configuration in this case; presumably a much slower sweep in  $\lambda$  would succeed. However, we believe that the results for  $n=2$  at this frequency should be essentially identical to the  $\omega=0$  case. The discrepancy between the MC results and the  $\omega=0$  results here are due to the finite  $\Delta\tau$  used in the MC simulation ( $\Delta\tau=0.5$  in this case).

As  $\omega$  is increased the  $n=2$  results also start to deviate somewhat from the  $\omega=0$  values. Note, however, that the system is much more insensitive to quantum fluctuations than the  $n=1$  case. For  $\omega=1.1$ , the results are still very close to the  $\omega=0$  results over almost all the  $\lambda$  range. For  $\omega=2$ , it appears that the order parameter does go to zero around  $\lambda=0.6$ . We believe however that the order parameter has just become too small to be noticed in Fig. 5(c), and that the system is ordered for all  $\lambda$ . We will return to this case later in this section.

In Fig. 6 we show results for the phonon order parameter versus frequency for the cases  $\lambda=0.9$  for  $n=1$  and  $\lambda=0.9/\sqrt{2}$  for  $n=2$ . The phonon order parameter has been normalized so that the values for  $n=1$  and 2 coincide at  $\omega=0$ . The system was started in the dimerized configuration and at each point 4000 measurements separated by two sweeps were

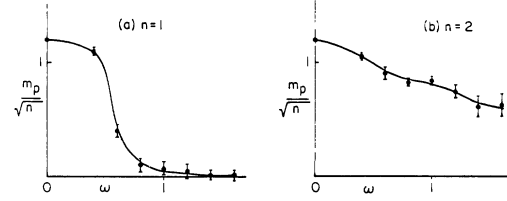


FIG. 6. Phonon order parameter vs phonon frequency. (a)  $n=1$ ,  $\lambda=0.9$ . (b)  $n=2$ ,  $\lambda=0.9/\sqrt{2}$ .

made. Then  $\omega$  was changed slowly until the next frequency point with  $\Delta\omega=0.002$  and 1 sweep per point. This was done to make sure that the system always remained in equilibrium. The difference between  $n=1$  and 2 is here most apparent. For  $n=1$ , there appears to be a transition to a disordered state around  $\omega=1$ , while the order parameter for  $n=2$  decreases slowly but does not vanish in the frequency range studied. This is in qualitative agreement with the strong coupling results in Sec. IV.

In Figs. 7 and 8 we show the phonon staggered correlation function

$$D_p(l) = \frac{1}{N} \sum_j (-1)^l \langle q_j q_{j+l} \rangle \quad (5.2)$$

and the electron staggered correlation function

$$D_e(l) = \frac{1}{N} \sum_{j,\sigma,\sigma'} (-1)^l (\langle n_{j\sigma} n_{j+l,\sigma'} \rangle - \langle n_{j\sigma} \rangle \langle n_{j+l,\sigma'} \rangle) \quad (5.3)$$

for  $n=1$  and 2,  $\lambda=0.9/\sqrt{n}$  and  $\omega=0$ ,  $\omega=0.4$ , and  $\omega=1.2$ . As expected, for the case  $n=1$  (Fig. 7) the correlations decay to zero for  $\omega=1.2$ , indicating that the system is disordered. Note the large value of  $D_p(l=0)$  for  $\omega=1.2$ . The on-site phonon correlations diverge as  $\omega \rightarrow \infty$ . For the case  $\omega=0.4$  there is a small reduction from the  $\omega=0$  value. The electronic correlations decay rapidly to their asymptotic value, which is nonzero for  $\omega=0$  and 0.4, indicating a site CDW. In the case  $n=2$  (Fig. 8) there is a gradual reduction in the correlations as  $\omega$  increases, but here fluctuations are greatly suppressed due to the larger number of fermion species. Even the on-site phonon correlation  $D_p(l=0)$  increases more slowly with  $\omega$  than for  $n=1$ . Note also that here the electronic on-site correlations  $D_e(l)$  do not go to the same value for all  $\omega$ , as happened for  $n=1$ . The reason is that  $D_e(l=0)$  has a piece proportional to  $\langle n_{j\uparrow} n_{j\downarrow} \rangle$ , which becomes smaller as  $\omega$  increases [in the case  $n=1$ ,  $D_e(l=0) = \langle n_j \rangle - \langle n_j \rangle^2 = 0.25$  independent of  $\omega$ ].

We now discuss in some more detail the case

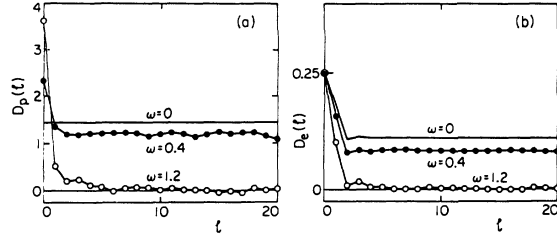


FIG. 7. Correlation functions vs distance for  $n=1$ ,  $\lambda=0.9$ , and three values of  $\omega$ . (a) Phonon-staggered correlation function. (b) Electron-staggered correlation function.

$n=1$ . Since we are dealing here with an infinite-order phase transition (at least we know this is the case in strong coupling), it is more difficult to see a clear signal of the transition than in an ordinary second-order transition since the correlation length diverges exponentially fast. A weak signal of the transition can be obtained from looking at the electronic static staggered susceptibility, defined as

$$\chi_f = \frac{1}{N} \sum_{i,j} (-1)^{i-j} (\langle n_i n_j \rangle - \langle n_i \rangle \langle n_j \rangle). \quad (5.4)$$

Figure 9 shows this quantity as a function of  $\lambda$  for the case  $\omega=1.1$ . Note that a weak peak appears at what we believe is the phase transition point  $\lambda \sim 1$ . A similar peak was observed in numerical simulations of the  $XXZ$  model.<sup>22</sup> The peak occurs because density-density correlation functions decay as  $1/R$  at the transition point; the peak in  $\chi_f$  in Eq. (2.4) should diverge logarithmically with the size of the system. For comparison, we show in Fig. 9 also the results in the static limit. Here, there is no peak and  $\chi_f$  starts to decrease when the long-range order becomes appreciable (the discrepancy between the MC and exact results at  $\lambda=0$  is due to the finite  $\Delta\tau$  used). For much smaller  $\omega$  we do not observe any peak in  $\chi_f$  and the curve resembles more the  $\omega=0$  results. We believe, however, that this is due to the effect of irrelevant operators and that  $\chi_f$  should show a divergence at the transition point for arbitrary

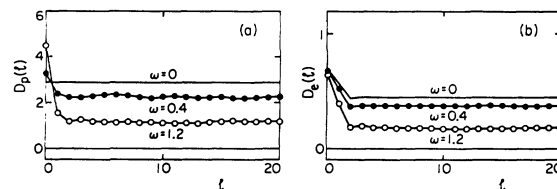


FIG. 8. Correlation functions vs distance for  $n=2$ ,  $\lambda=0.9/\sqrt{2}$ , and three values of  $\omega$ . (a) Phonon-staggered correlation function. (b) Electron-staggered correlation function.

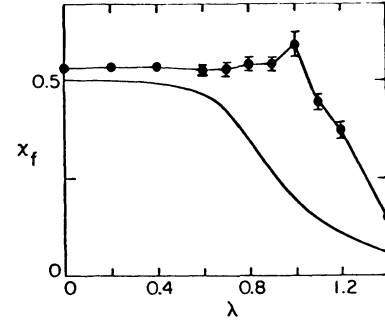


FIG. 9. Electronic staggered susceptibility vs  $\lambda$  for  $n=1$  and  $\omega=1.1$ . For comparison the exact  $\omega=0$  results are also shown.

rary  $\omega$  in a sufficiently large system.

In Fig. 10 we show the spatial decay of the fermion density-density correlation function in a double-logarithmic plot for the case  $\omega=1.1$ ,  $\lambda=1.0$ . The dashed line shows the behavior for  $\lambda=0$  on the finite lattice, which is close to  $1/R^2$  decay. The MC results show a markedly slower rate of decay closer to  $1/R$ , as we expect at the transition point. The oscillations between even and odd  $l$  occur also for the noninteracting case, in fact, there  $D_e(l)$  is identically zero for  $l$  even.

In Fig. 11 we collect the results of several runs in a phase diagram for the case  $n=1$ . The MC results for the phase-transition points were obtained from estimating where the order parameter or the staggered correlation functions vanished and from results for the fermion susceptibility for large  $\omega$ . The error bars are an estimate on the error in this procedure. The dashed line is the result of the strong coupling expansion, Eq. (4.11). The MC results appear to differ somewhat even for the largest frequency studied,  $\omega=2$ . This is probably due to the fact

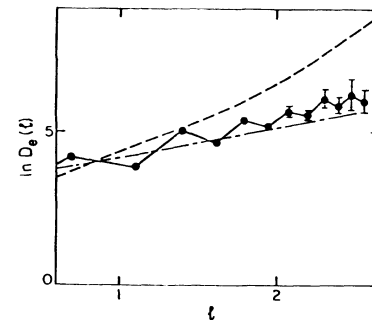


FIG. 10. Spatial decay of fermion correlation function  $D_e(l)$  is plotted vs  $l$  in a double-logarithmic plot for  $n=1$ ,  $\omega=1.1$ , and  $\lambda=1$ . Dashed lines are exact results for the case  $\omega=0$  which follows a  $1/l^2$  behavior. Dashed-dotted line shows  $1/l$  behavior.

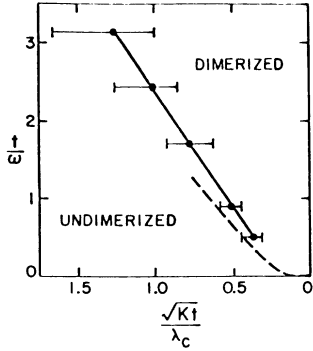


FIG. 11. Phase diagram for the molecular-crystal model for  $n=1$ . Dashed line is the strong coupling results [Eq. (4.11)].

that in the strong coupling results we have neglected the effect of the second-nearest-neighbor term in Eq. (4.8). For  $\omega=2$ ,  $t_2/t=0.27$ , it only becomes negligible for larger  $\omega$ . For small  $\omega$ , it becomes very difficult to identify the location of the transition point from the MC data, since  $\lambda_c$  becomes small and the order parameter even for the case  $\omega=0$  becomes very small. We expect, however, the phase-transition line to join smoothly the static limit values  $\omega=0$ ,  $\lambda_c=0$ . We believe the transition between dimerized and undimerized states is always of infinite order, although we have analytic and numerical evidence only for large  $\lambda_c$ .

We now discuss in more detail the case  $n=2$ . As mentioned earlier in Fig. 5(c) it appears that the order parameter vanishes around  $\lambda=0.6$  for  $\omega=2$ . However, this can be also just an indication that the correlation length has become larger than the lattice and the system merely *appears* disordered for the finite lattice. In order to shed light on this question we have used a finite-size-scaling analysis, which can give us information about the infinite system even for parameters where the correlation length is larger than the lattices under consideration. The finite-size-scaling hypothesis<sup>23</sup> states that the gap for a finite system of  $N$  sites  $\Delta_N$  can be written as<sup>24,25</sup>

$$\Delta_N = \frac{1}{N} f(N\Delta_\infty), \quad (5.5)$$

with  $\Delta_\infty$  the gap for the infinite lattice. The validity of Eq. (5.5) has been demonstrated analytically for the Ising model in  $1+1$  dimensions<sup>24</sup> and numerically (from diagonalization of finite systems) for several other models.<sup>25</sup> Here we will use a graphical procedure which we believe is the most appropriate if one has statistical errors (a direct calculation of the  $\beta$  function does not give good results in this

case). If the gap has the analytic form

$$\Delta_\infty = c e^{-aKt/\lambda^2} \quad (5.6)$$

given a system of size  $N_1$  at coupling constant  $\lambda_1$  and another of size  $N_2$  at coupling constant  $\lambda_2$  such that

$$N_1 \Delta_{N_1}(\lambda_1) = N_2 \Delta_{N_2}(\lambda_2), \quad (5.7)$$

one obtains from (5.5) and (5.7):

$$\frac{Kt}{\lambda_1^2} - \frac{Kt}{\lambda_2^2} = \frac{1}{a} \ln(N_1/N_2). \quad (5.8)$$

Thus Eq. (5.8) gives us information about the behavior of the gap and the constant in the exponent of Eq. (5.6) even in regions where the correlation length is larger than the lattice. We have chosen to study small systems and runs long enough to obtain good statistics. Since it is difficult to obtain the gap directly from the MC simulation we extracted it from the phonon order parameter through the relation  $\Delta = \lambda m_p$ . This holds in the case  $\omega=0$  and also in perturbation theory to one-loop order. Even the phonon order parameter cannot be obtained directly for small systems, since the system will tunnel frequently between the two ground states and the average  $m_p$  will vanish. We considered therefore the phonon time-correlation function

$$G_p(\tau) = \langle O_p(\tau) O_p(0) \rangle, \quad (5.9)$$

with

$$O_p = \frac{1}{N} \sum_j (-1)^j q_j \quad (5.10)$$

and  $O_p(\tau) = e^{H\tau} O_p e^{-H\tau}$ . In the noninteracting case this function is

$$G_p^0(\tau, \omega) = \frac{1}{2NM\omega} e^{-\omega\tau} \left[ 1 + \frac{e^{2\omega\tau} + 1}{e^{\beta\omega} - 1} \right]. \quad (5.11)$$

For the interacting case, this function was fitted to

$$G_p(\tau) = G_p^0(\tau, \bar{\omega}) + m_p^2, \quad (5.12)$$

and from here the phonon order parameter was extracted. Figure 12 shows phonon time-correlation functions on a  $16 \times 16$  lattice for  $\omega=2$  and various  $\lambda$ 's. Note that the renormalized frequency  $\bar{\omega}$  first *decreases* and then increases again as  $\lambda$  is increased [for  $\lambda=1$  (not shown in Fig. 13),  $\omega=1.5$ ]. Within mean-field theory  $\bar{\omega}$  is an *increasing* function of  $\lambda$  and goes to 0 as  $\lambda \rightarrow 0$ , independent of  $\omega$ . (Of course, for small  $\lambda$  anharmonic effects must become dominant in the phonon behavior within mean-field theory.<sup>26</sup>)

In Fig. 13 we show results for  $\ln(N\Delta_N)$  obtained in the form described above for lattices of size

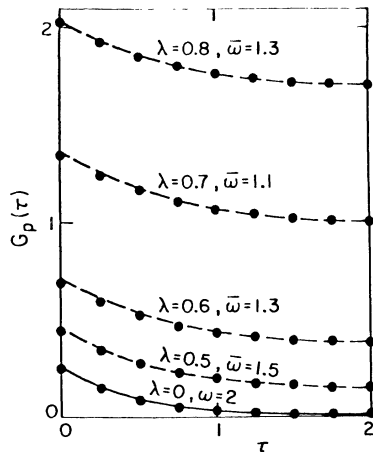


FIG. 12. Phonon order parameter time correlation function  $G_p(\tau)$  for the case  $n=2$ ,  $\omega=2$ , and several values of  $\lambda$  on a  $16 \times 16$  lattice. Dashed lines are fit to the form Eq. (5.12), the solid line is exact results for  $\lambda=0$ .

$N=L=8, 12$ , and  $16$ , for  $\omega=2$  and  $0$ . We have done very long runs, particularly for small  $\lambda$ 's (up to 40 000 measurements), and the statistical errors are of order of the size of the points where not shown. According to Eq. (5.6) we should obtain straight lines of slope  $1/a$ , but of course that is not the case because of finite-size effects. However, from Eqs. (5.7) and (5.8) we see that the horizontal distance between the curves should give us the value of  $a$ . The horizontal bars in Fig. 13(b) show the expected distance in the static limit ( $a=\pi$ ) and it can be seen that the agreement is very good. In the case  $\omega=2$  the curves are steeper and closer together, which in-

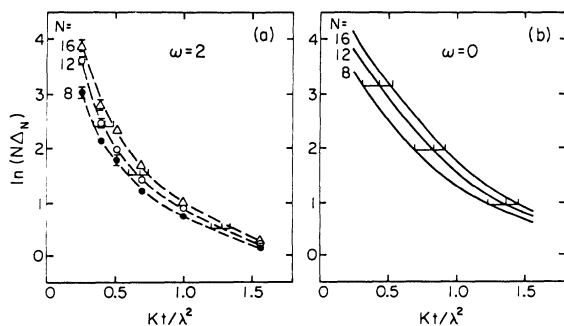


FIG. 13. Finite-size-scaling analysis of the case  $n=2$ . Logarithm of the lattice size times the gap is plotted vs  $Kt/\lambda^2$  for the cases (a)  $\omega=2$  and (b)  $\omega=0$ . Note that the curves are steeper and closer in (a) than (b), but they do not come together. Horizontal bar in (b) is the expected distance between curves in the  $\omega=0$  limit [Eq. (5.8)] with  $a=\pi$ . Horizontal bars in (a) represent the distance given by Eq. (5.8) with  $a=5$ .

dicates a larger value for  $a$ . However, they *do not* come together, which would be the case if a phase transition occurs, and  $\Delta_\infty$  vanishes<sup>25</sup> [see Eq. (5.5)]. The distance between the curves appears to be approximately constant with  $\lambda$  and corresponds approximately to  $a=5$  [shown as horizontal bars in Fig. 13(a)]. Thus Fig. 13 gives us fairly strong evidence that the system does not disorder for  $\lambda \sim 0.6$ , as could have been inferred from the results of Fig. 5(c). From all the numerical evidence we conclude that the system for  $n=2$  is probably dimerized for arbitrary  $\lambda$  as long as  $\omega$  is not infinite.

## VI. SUMMARY AND CONCLUSIONS

We have studied the nature of the ground state in the one-dimensional molecular-crystal model as a function of phonon frequency and electron-phonon coupling constant. For the case of spinless electrons the analytic strong coupling results and the numerical results indicate that there is a phase transition between a disordered and a Peierls-dimerized state at a critical coupling  $\lambda_c(\omega)$ . We have the analytic results  $\lambda_c(\omega=0)=0$ ,  $\lambda_c(\omega=\infty)=\infty$ , and an analytic form for  $\lambda_c(\omega)$  in strong coupling. The numerical results approach the strong coupling results for large  $\omega$ . Although we have not direct evidence for small  $\omega$ , it is reasonable to assume that  $\lambda_c(\omega)$  defines a continuous curve in the  $\lambda$ - $\omega$  plane from  $\lambda_c(0)=0$  to  $\lambda_c(\infty)=\infty$ . We have evidence that the transition is of infinite order both for strong coupling and for  $\omega=0$  so that it is reasonable to conclude that this holds everywhere.

For the case  $n=2$  the numerical results appear to indicate that the system is ordered for all  $\omega < \infty$ . The analytic results in strong coupling confirm this. Exactly at  $\omega=\infty$ , however, the system is at the critical point and is disordered. We have seen that this is due to a continuous symmetry of the model, which is broken for any  $\omega < \infty$ . Thus it is reasonable to assume that the system is dimerized for all couplings for  $\omega < \infty$ . We believe that it is possible to prove this analytically in weak coupling from a RG analysis and work is in progress in that direction. It appears, however, that retardation effects play a role only at two-loop order, so that the calculation is nontrivial.

The qualitatively different behavior between the cases  $n=1$  and  $2$  is perhaps somewhat surprising since they are identical within the mean-field approximation. It is satisfying, however, that one can understand this difference from various different viewpoints. From the point of view of the strong coupling expansion the difference appears because the small polarons can hop in first order but interact only in second order for  $n=1$ , while they hop and

interact only in second order for  $n=2$ . From the point of view of the MC simulation the difference can be seen in that having a single electron hop has a ratio of matrix elements  $\tanh\Delta\tau t$ , while having a pair of electrons of opposite spins hop costs  $(\tanh\Delta\tau t)^2$ . Thus the system for  $n=2$ , where the electrons are mostly paired, has a more difficult time disordering than the case  $n=1$ . Finally, from the point of view of weak coupling perturbation theory the difference is of course that the system with  $n=2$  can undergo umklapp scattering for two electrons of opposite spin at the Fermi surface, while this is suppressed in the case  $n=1$  due to the Pauli exclusion principle.

As mentioned earlier, systems like the one discussed here can also display superconducting correlations. For the case studied in this paper the Peierls instability dominates even at high oscillator frequency. Although the electrons are always paired, there is long-range CDW order and superconducting correlation decay exponentially. Only at  $\omega = \infty$  there is coexistence of long-range superconducting and CDW correlations. This situation is, however, modified if the non-half-filled-band case is considered or if longer-range coupling between electrons and phonons is introduced. A systematic study of this and related models in regimes where

superconductivity dominates will be the subject of a forthcoming paper.<sup>27</sup>

As discussed in Ref. 1, a possible physical realization of the case  $n=1$  could occur in the presence of a strong magnetic field. Another example is a quarter-filled-band system with a strong on-site Hubbard repulsion; this is equivalent to the spinless half-filled-band case considered in this paper. A possible experimental realization of this system could be provided by the highly correlated 1:2 salts of TCNQ.<sup>28</sup> We hope that some of our predictions can be tested experimentally. In the future we plan to study more realistic models with the use of similar techniques, particularly including electron-electron interactions.

#### ACKNOWLEDGMENTS

One of us (J.H.) is grateful to D. Scalapino for raising his interest in this problem and for several stimulating conversations. We acknowledge helpful discussions with S. Kivelson, W. P. Su, R. Sugar, S. Shenker, J. Schrieffer, and D. Scalapino. One of us (E.F.) thanks the Institute for Theoretical Physics, Santa Barbara, for its kind hospitality. This work was supported by the National Science Foundation under Grants Nos. PHY-77-27084 and DMR-81-17182.

#### APPENDIX

We give here some details of the strong coupling expansion calculation of Sec. IV. For the spinless case, the second-order Hamiltonian has a nearest-neighbor (NN) and a next-nearest-neighbor (NNN) term. The first arises from processes where an electron hops to a neighboring site and back to the same site, and is of the form

$$H_2^1 = \frac{2t^2}{\omega} \left[ \sum_{n,n' \neq (0,0)} \frac{|\langle -0 | +n \rangle|^2 |\langle +0 | -n' \rangle|^2}{n+n'} \right] \sum_i \tilde{n}_i \tilde{n}_{i+1}. \quad (\text{A1})$$

Note that this process gives a *repulsive* interaction between polarons since it is allowed only if the neighboring site is empty. In (A1) we have omitted chemical-potential terms. The NNN term is of the form

$$H_2^2 = \frac{t^2}{\omega} |\langle -0 | +0 \rangle|^2 \left[ \sum_{n \neq 0} \frac{|\langle +0 | -n \rangle|^2}{n} \right] \sum_i [\tilde{C}_{i+1}^\dagger (1 - \tilde{n}_i) \tilde{C}_{i-1} + \text{H.c.}]. \quad (\text{A2})$$

The phonon matrix elements can be evaluated exactly and yield

$$\langle +0 | -n \rangle = \frac{(2g)^{n/2} e^{-g}}{(n!)^{1/2}}, \quad (\text{A3a})$$

$$\langle -0 | +n \rangle = (-1)^n \langle +0 | -n \rangle, \quad (\text{A3b})$$

with  $g$  given in Eq. (4.5). We obtain then from (A1) for the magnitude of the interactions between polarons,

$$\tilde{v} = \frac{2t^2}{\omega} e^{-4g} \sum_{(n,n') \neq (0,0)} \frac{(2g)^n (2g)^{n'}}{n! n'} \frac{1}{n+n'}, \quad (\text{A4})$$

which can be rewritten as the integral given by Eq. (4.9a). The NNN term gives, from (A2),

$$\tilde{t}_2 = \frac{t^2}{\omega} \sum_{n \neq 0} \frac{(2g)^n}{n!} \frac{1}{n}, \quad (\text{A5})$$

or equivalently Eq. (4.9b).

For the case with spin, the two second-order processes involve only NN sites. The processes where one electron hops to the neighboring site and back to the same site yields

$$H_2^1 = \frac{4t^2}{\omega} \left[ \sum_{n,n'} \frac{|\langle +0|n\rangle|^2 |\langle -0|n'\rangle|^2}{n+n'+4g} \right] \sum_i \tilde{n}_i \tilde{n}_{i+1}. \quad (\text{A6})$$

Here,  $|+0\rangle, |-0\rangle$  denotes the ground state of the oscillator with equilibrium position  $\pm q_0$ , with  $q_0 = \lambda/K$ , respectively, and  $|n\rangle$  denotes the  $n$ th excited state of the oscillator centered at  $q=0$ . The intermediate states involve singly occupied sites. Note that the sum in Eq. (A6) includes now the term  $n=n'=0$ .

The second type of process involves an electron hopping to the neighboring site, and then the second electron follows. This gives a NN hopping term for the pairs of the form

$$H_2^2 = \frac{2t^2}{\omega} \sum_{n,n'} \left[ \frac{\langle +0|n\rangle \langle n|-0\rangle \langle -0|n'\rangle \langle n'|+0\rangle}{n+n'+4g} \right] \sum_i (\tilde{b}_i^\dagger \tilde{b}_{i+1} + \text{H.c.}). \quad (\text{A7})$$

The matrix elements are again given by Eq. (A3) (with  $|n\rangle$  replacing  $|+n\rangle, |-n\rangle$ ). Note that the hopping term (A7) will have a factor  $(-1)^{n+n'}$  which is absent in the interaction term. Owing to this the interaction term always dominates. From (A6) and (A7), Eq. (4.14) follows.

---

\*Present address: Department of Physics, University of California, San Diego, La Jolla, CA 92093.

<sup>1</sup>E. Fradkin and J. E. Hirsch, Phys. Rev. B **27**, 1680 (1983).

<sup>2</sup>T. Holstein, Ann. Phys. **8**, 325 (1959).

<sup>3</sup>W. A. Little, Phys. Rev. **134**, A1416 (1964).

<sup>4</sup>R. E. Peierls, in *Quantum Theory of Solids* (Oxford University Press, London, 1955), p. 108.

<sup>5</sup>W. P. Su, J. R. Schrieffer, and A. J. Heeger, Phys. Rev. B **22**, 2099 (1980).

<sup>6</sup>E. Conwell, Phys. Rev. B **22**, 1761 (1980).

<sup>7</sup>D. K. Campbell, A. R. Bishop, and E. Fesser (unpublished).

<sup>8</sup>F. D. M. Haldane, Phys. Rev. Lett. **45**, 1358 (1980).

<sup>9</sup>J. L. Black and V. J. Emery, Phys. Rev. B **23**, 429 (1981).

<sup>10</sup>M. P. M. den Nijs, Phys. Rev. B **23**, 6111 (1981).

<sup>11</sup>T. Holstein, Ann. Phys. **8**, 343 (1959).

<sup>12</sup>G. Beni, P. Pincus, and J. Kanamore, Phys. Rev. B **10**, 1896 (1974).

<sup>13</sup>A. Luther and I. Peschel, Phys. Rev. B **12**, 3908 (1975).

<sup>14</sup>J. E. Hirsch, D. J. Scalapino, R. L. Sugar, and R. Blankenbecler, Phys. Rev. Lett. **47**, 1628 (1981); see also Phys. Rev. B **26**, 5033 (1982).

<sup>15</sup>J. E. Hirsch and E. Fradkin, Phys. Rev. Lett. **49**, 402

(1982).

<sup>16</sup>D. J. Scalapino and R. L. Sugar, Phys. Rev. B **24**, 4295 (1981).

<sup>17</sup>V. J. Emery, in *Highly Conducting One-dimensional Solids*, edited by J. Devreese, R. Evrard, and V. van Doren (Plenum, New York, 1979).

<sup>18</sup>E. Lieb and F. Wu, Phys. Rev. Lett. **20**, 1445 (1968).

<sup>19</sup>N. Mermin and H. Wagner, Phys. Rev. Lett. **17**, 1133 (1966).

<sup>20</sup>E. Lieb, T. Schultz, and D. Mattis, Ann. Phys. **16**, 407 (1961).

<sup>21</sup>V. J. Emery, Phys. Rev. B **14**, 1989 (1976).

<sup>22</sup>J. E. Hirsch (unpublished).

<sup>23</sup>M. E. Fisher and M. N. Barber, Phys. Rev. Lett. **28**, 1516 (1972).

<sup>24</sup>C. Hamer and M. Barber, J. Phys. A **14**, 241 (1981).

<sup>25</sup>H. H. Roomany and H. W. Wyld, Phys. Rev. D **21**, 3341 (1980).

<sup>26</sup>We are grateful to S. Kivelson for discussion on this point.

<sup>27</sup>J. E. Hirsch and D. J. Scalapino (unpublished).

<sup>28</sup>M. J. Rice and E. J. Mele, Phys. Rev. B **25**, 1339 (1982). We are grateful to M. Rice for pointing this out to us.